Density Functional Theory and Ab Initio Direct Dynamics Studies on the Hydrogen Abstraction Reactions of $SiH_{4-n}(CH_3)_n + H \rightarrow SiH_{3-n}(CH_3)_n + H_2$, $n = 1-3$

Xin Yu,[†] Shen-Min Li,[†] Zhen-Feng Xu,[‡] Ze-Sheng Li,*[,†] and Chia-Chung Sun[†]

Institute of Theoretical Chemistry, State Key Laboratory of Theoretical and Computational Chemistry, Jilin University, Changchun 130023, People's Republic of China, and Department of Applied Chemistry, Beijing University of Chemical Technology, Beijing 100029, People's Republic of China

Received: November 7, 2000; In Final Form: April 11, 2001

Density functional theory (DFT) and ab initio direct dynamics methods have been used to study three hydrogen abstraction reactions of $SiH_{4-n}(CH_3)_n + H \rightarrow SiH_{3-n}(CH_3)_n + H_2$, $n = 1-3$. For all the reactions, the potential energy surface information is calculated at the DFT BHLYP/6-311+G** level, and energies along the minimum energy path are improved by a series of single-point ab initio PMP4/6-311+G(3df,2p)//BHLYP calculations. Changes of geometries, generalized normal-mode vibrational frequencies, and potential energies along the reaction path of the reactions are discussed and compared. The rate constants of the reactions are calculated by canonical variational transition state theory with the small-curvature tunneling correction (CVT/SCT) method in the temperature range 290−3000 K. Good agreement with experimental values is found for rate constants over the measured temperature ranges. The results show that the variational effect is small and, in the lower temperature range, the small curvature tunneling effect is important for the reactions. Methyl substitution increases the reactivity of the Si−H bond toward H atom attack, and the increase in k/n mainly stems from a corresponding increase in A/n. The activation energies for the three methyl-substituted silane reactions are nearly the same. Three-parameter fits for rate constants of the reactions within 290−3000 K are presented.

Introduction

The effect of the replacement of H by CH_3 on the reactivity of the Si−H bond in SiH_4 is a subject of many experimental studies.[1−9] A number of investigations involving attack by different atoms and free radicals: Cl,[1,2] Br,[1,2] I,[3] CF_3,[4] CH_3,[4] O,[5] and H[6−9] have been reported. The effect observed varies markedly from one attacking species to another. Reactions of hydrogen atoms, the simplest free radical species, are of particular interest since these reactions provide an uncomplicated probe of chemical reactivity. Among the four most recent experimental investigations[6−9] about H atoms with different methlysilanes, the work by Austin and Lampe,[6] indicated that successive methyl substitution leads to increases in k/n (rate constant corrected for reaction path degeneracy), and they attributed it solely to the changes in activation energy. The same trend of k/n had been observed by Arthur, Potzinger, and co-workers,[7] but they thought the predominant contribution to the change in rate constant is a corresponding change in A-factor (preexponential factor of Arrhenius equation). To reconcile the conflict between the results of previous work and obtain dependable rate constants over a wide temperature range, Arthur and Miles made two further studies on the reactions of H atoms with the methylsilanes, at room temperature[8] and 298−580 K,[9] respectively. The results they obtained were similar to those of Arthur, Potzinger, and co-workers.[7] But for the low activation energy for $SiH(CH_3)_3$, the explanation was different. Arthur, Potzinger, and co-workers[7] interpreted that the activation energies for hydrogen attack on the methylsilanes were essentially equal within experimental error, any differences being due to experimental scatter. However, according to Arthur and Miles,[9] the low activation energy for attack on $SiH(CH_3)_3$ was a real effect, and not merely the result of experimental scatter.

Our objective in embarking on the present work is to make a systematic theoretical survey on the hydrogen abstraction reactions of $SiH_{4-n}(CH_3)_n + H \rightarrow SiH_{3-n}(CH_3)_n + H_2$, $n = 1-3$, to provide calculational results for the reaction path and rate constant, and to explore the effect of methyl substitution on the reactivity of the Si−H bond. Little theoretical attention has been paid to the reactions to our knowledge.

The DFT and ab initio direct dynamics method developed by Truong and co-workers[10−16] have been used to study the reactions. This method can reduce the demand of calculational resources without sacrificing the accuracy of rate constants and has been successfully applied to some chemical reaction dynamical studies. Recently, we have employed this method to study two hydrogen abstraction reactions[17,18] and have obtained satisfactory rate constants. It is expected that this method is applicable to the present reactions.

Calculational Methods

The direct dynamics method[19] uses electronic structure information, including geometries, energies, gradients, and force constants (Hessians) at selected points on the reaction path, to calculate rate constants without the intermediate stage of constructing a full analytical potential energy surface. The present study is carried out in two stages: in the first stage, by means of the GAUSSIAN98 program,[20] DFT and ab initio calculations are carried out for stationary points (reactant, transition state, and product) and for the minimum energy path (MEP) to obtain electronic structure information for the reactions. The method of DFT BHLYP (the combination of Becke's

* Corresponding author. Fax: +86-431-8945942. E-mail: itcjlu@public.cc.jl.cn.
[†] Jilin University.
[‡] Beijing University of Chemical Technology.

10.1021/jp004087m CCC: $20.00
Published on Web 06/28/2001

TABLE 1: Geometrical Parameters (Distances in Angstroms and Angles in Degrees) of the Equilibrium and Transition-State Structures for the Reactions at the BHLYP/6-311+G Level[a]**

molecule	symmetry	*R*(HH)	*R*(SiC)	*R*(SiH)	*R*(SiH′)	*R*(H′H″)	∠HSiH	∠HSiC	∠CSiC	∠HSiH′	∠SiH′H″
H_2	$D_{\infty h}$	0.7383 (0.7414)									
SiH_3CH_3	C_{3v}		1.8730 (1.867)	1.4779 (1.485)			108.3338 (108.3)	110.5860			
SiH_2CH_3	C_s		1.8780	1.4803			109.5117	111.7207			
SiH_2CH_3-H′-H″ (TS)	C_s		1.8722	1.4780	1.5874	1.1651	109.1573	111.4443		107.4827	180
$SiH_2(CH_3)_2$	C_{2v}		1.8744	1.4808			107.5414	109.4492	111.4196		
$SiH(CH_3)_2$	C_s		1.8804	1.4844				110.1723	111.7664		
$SiH(CH_3)_2$- H′-H″ (TS)	C_s		1.8733	1.4809	1.5991	1.1453		110.3480	112.2647	107.0055	177.4555
$SiH(CH_3)_3$	C_{3v}		1.8761	1.4837				108.5599	110.3670		
$Si(CH_3)_3$	C_{3v}		1.8824						110.4371		
$Si(CH_3)_3$- H′-H″ (TS)	C_{3v}		1.8749		1.6128	1.1247			111.2293		180

[a] The values in parentheses are experimental values from ref 24.

TABLE 2: Harmonic Vibrational Frequencies (cm^{-1}) of the Equilibrium and Transition-State Structures for the Reactions at the BHLYP/6-311+G Level[a]**

molecule	frequency					
H_2	(Σ_g^+)4519 (4403)					
SiH_3CH_3	(A2)196	(E)539	(A1)715	(E)922	(A1)987	(E)1001
	(187)	(540)	(700)	(868)	(940)	(980)
	(A1)1351	(E)1514	(E)2285	(A1)2290	(A1)3114	(E)3190
	(1260)	(1403)	(2166)	(2169)	(2898)	(2982)
SiH_2CH_3	(A″)179	(A″)544	(A′)595	(A′)709	(A′)881	(A″)922
	(A′)972	(A′)1341	(A″)1506	(A′)1510	(A′)2253	(A″)2273
	(A′)3104	(A′)3176	(A″)3196			
SiH_2CH_3-H′-H″ (TS)	(A″)156	(A′)182	(A″)314	(A″)549	(A′)603	(A′)715
	(A′)913	(A″)923	(A′)985	(A′)1011	(A″)1020	(A′)1202
	(A′)1349	(A″)1511	(A′)1512	(A′)2280	(A″)2286	(A′)3113
	(A′)3187	(A″)3193	(A′)998*i*			
$SiH_2(CH_3)_2$	(A2)154	(B1)173	(A1)213	(B1)482	(A2)606	(B2)670
	(A1)671	(B2)743	(A1)895	(B1)921	(A2)926	(B2)967
	(A1)1007	(B2)1345	(A1)1352	(A2)1508	(B2)1510	(A1)1516
	(B1)1520	(B1)2262	(A1)2270	(B2)3107	(A1)3108	(A2)3180
	(B1)3182	(A1)3183	(B2)3184			
$SiH(CH_3)_2$	(A″)134	(A′)151	(A′)208	(A′)528	(A″)636	(A′)659
	(A″)715	(A″)757	(A′)897	(A′)907	(A″)934	(A″)1335
	(A′)1342	(A″)1501	(A″)1505	(A′)1509	(A′)1515	(A′)2234
	(A″)3096	(A′)3097	(A″)3168	(A′)3169	(A″)3190	(A′)3191
$SiH(CH_3)_2$−H′−H″ (TS)	(A″)144	(A′)155	(A″)175	(A′)191	(A′)213	(A′)545
	(A″)635	(A′)666	(A″)703	(A″)752	(A′)894	(A′)913
	(A″)933	(A″)1004	(A′)1017	(A′)1166	(A″)1343	(A′)1350
	(A″)1506	(A″)1507	(A′)1513	(A′)1518	(A′)2263	(A″)3106
	(A′)3107	(A″)3178	(A′)3179	(A″)3187	(A′)3188	(A′)977*i*
$SiH(CH_3)_3$	(A2)152	(E)167	(E)210	(A1)248	(A1)634	(E)644
	(A2)711	(E)728	(E)885	(A1)910	(E)955	(E)1344
	(A1)1354	(A2)1504	(E)1508	(E)1517	(A1)1525	(A1)2248
	(E)3103	(A1)3104	(E)3174	(A1)3176	(A2)3178	(E)3179
$Si(CH_3)_3$	(A2)141	(E)153	(E)206	(A1)233	(A1)617	(E)706
	(A2)719	(E)748	(E)898	(A1)903	(E)1333	(A1)1345
	(A2)1497	(E)1505	(E)1510	(A1)1522	(E)3089	(A1)3090
	(E)3162	(A1)3163	(A2)3187	(E)3188		
$Si(CH_3)_3$−H′−H″ (TS)	(A2)140	(E)152	(E)169	(E)210	(A1)235	(A1)625
	(E)700	(A2)716	(E)739	(E)893	(A1)897	(E)1002
	(A1)1124	(E)1342	(A1)1353	(A2)1500	(E)1506	(E)1513
	(A1)1523	(E)3102	(A1)3103	(E)3172	(A1)3174	(A2)3183
	(E)3184	(A1)965*i*				

[a] The values in parentheses are experimental values from ref 25.

half-and-half (BH) exchange functional with Lee−Yang−Parr (LYP) correlation functional) and the 6-311+G** basis set are used to optimize the geometries and frequencies of the stationary points. Then at the same level, the MEP is obtained by the intrinsic reaction coordinate (IRC) method with a gradient step size of 0.05 $(amu)^{1/2}$ bohr in mass-weighted Cartesian coordinates, and the harmonic vibrational frequencies as well as the force-constant matrices at the selected points along the MEP are calculated. Finally, the ab initio spin-projected fourth-order Moller−Plesset perturbation theory (PMP4) is performed using a larger 6-311+G(3df,2p) basis set (PMP4/6-311+G(3df,2p)) to refine the energies of selected points along the MEP. In the second stage, the electronic structure information for the reactions is input into POLYRATE-Version 8.4.1[21] to calculate variational transition state theory rate constants and their temperature dependence. Canonical variational transition state theory (CVT) rate constants are calculated with the small-curvature tunneling (SCT) correction method proposed by Truhlar and co-workers.[22,23] During the calculation, the Euler-with-stabilization integrator with a step size of 0.0001 $(amu)^{1/2}$

TABLE 3: Reaction Enthalpies (ΔH^0_{298}) and Potential Barriers (ΔE) (kcal/mol) for the Reactions[a]

	BHLYP		PMP4//BHLYP	
reaction	ΔH^0_{298}	ΔE	ΔH^0_{298}	ΔE
$SiH_3CH_3 + H \rightarrow SiH_2CH_3 + H_2$[b]	−11.89	2.36	−11.38	4.84
$SiH_2(CH_3)_2 + H \rightarrow SiH(CH_3)_2 + H_2$[c]	−11.00	2.13	−10.37	4.50
$SiH(CH_3)_3 + H \rightarrow Si(CH_3)_3 + H_2$[d]	−10.22	1.95	−9.50	4.21

[a] Total energies (in hartrees). [b] For $SiH_3CH_3 + H \rightarrow SiH_2CH_3 + H_2$, at BHLYP(ZPE): SiH_3CH_3, −331.131834; H, −0.498546; SiH_2CH_3, −330.490871; H_2, −1.159323; TS, −331.626615. At PMP4/6-311+G(3df,2p)//BHLYP: SiH_3CH_3, −330.615501; H, −0.499810; SiH_2CH_3, −329.974397; H_2, −1.159926; TS, −331.107597. [c] For $SiH_2(CH_3)_2 + H \rightarrow SiH(CH_3)_2 + H_2$, at BHLYP(ZPE): $SiH_2(CH_3)_2$, −370.413992; H, −0.498546; $SiH(CH_3)_2$, −369.771626; H_2, −1.159323; TS, −370.909146. At PMP4/6-311+G(3df,2p)//BHLYP: $SiH_2(CH_3)_2$, −369.838430; H, −0.499810; $SiH(CH_3)_2$, −369.195715; H_2, −1.159926; TS, −370.331061. [d] For $SiH(CH_3)_3 + H \rightarrow Si(CH_3)_3 + H_2$, at BHLYP(ZPE): $SiH(CH_3)_3$, −409.696705; H, -0.498546; $Si(CH_3)_3$, −409.053104; H_2, −1.159323; TS, −410.192139. At PMP4/6-311+G(3df,2p)//BHLYP: $SiH(CH_3)_3$, −409.0625395; H, −0.499810; $Si(CH_3)_3$, −408.41846; H_2, −1.159926; TS, −409.555636.

bohr is used to follow the MEP, and the generalized normal-mode analysis is performed every 0.01 $(amu)^{1/2}$ bohr. The curvature components are calculated using a quadratic fit to obtain the derivative of the gradient with respect to the reaction coordinate.

Results and Discussion

A. Stationary Points. Table 1 lists the geometrical parameters of the equilibrium and transition-state structures of the reactions at the BHLYP/6-311+G** level along with the available experimental data.[24] When comparison is possible, the optimized geometrical parameters of SiH_3CH_3 and H_2 are in good agreement with the experimental values. It might be inferred that the same accuracy could be expected for the other calculated geometries. In the transition-state structures, the length of the bond Si−H′ which will be broken increases by 7.4%, 8.0%, and 8.7% with respect to the Si−H equilibrium bond lengths of SiH_3CH_3, $SiH_2(CH_3)_2$, and $SiH(CH_3)_3$, respectively. The length of the H′−H″ bond that will form the hydrogen molecule is 1.58, 1.55, and 1.52 times, respectively, as large as the equilibrium bond length of the hydrogen molecule. Therefore, all of the transition states are reactant like, and the reactions will proceed via early transition states. This is the expected behavior from Hammond's postulate, since all of the reactions are exothermic. In addition, from $SiH(CH_3)_3$ to SiH_3CH_3, the transition state via which the reaction will proceed occurs earlier and earlier.

The harmonic vibrational frequencies of the equilibrium and transition-state structures of the reactions at the BHLYP/6-311+G** level are listed in Table 2 along with the available experimental data.[25] As can be seen, most of our calculated frequencies are in good agreement with those of the available experimental values, and the maximum error between them is about 8%. The imaginary frequency for the transition state of the reactions is 998, 977, and 965 cm^{-1}, respectively, which implies that the tunneling effect is similar for the reactions.

Table 3 lists the reaction enthalpies and potential barriers calculated at the BHLYP/6-311+G** and PMP4/6-311+G(3df,-2p)//BHLYP levels. From it one can see that the difference between the calculated reaction enthalpies (298 K) for each reaction is not large at the two levels. The maximum difference is found to be 0.72 kcal/mol for the reaction of H with $SiH(CH_3)_3$. Because of the absence of experimental standard heats of formation of the present reaction systems, it is difficult to make a conclusive comparison on reaction enthalpies. The obvious difference is found for the calculated potential-barrier height. For each reaction, the PMP4/6-311+G(3df,2p)//BHLYP increases the potential-barrier height at least by 2 kcal/mol in comparison with the BHLYP/6-311+G** method. The observa-

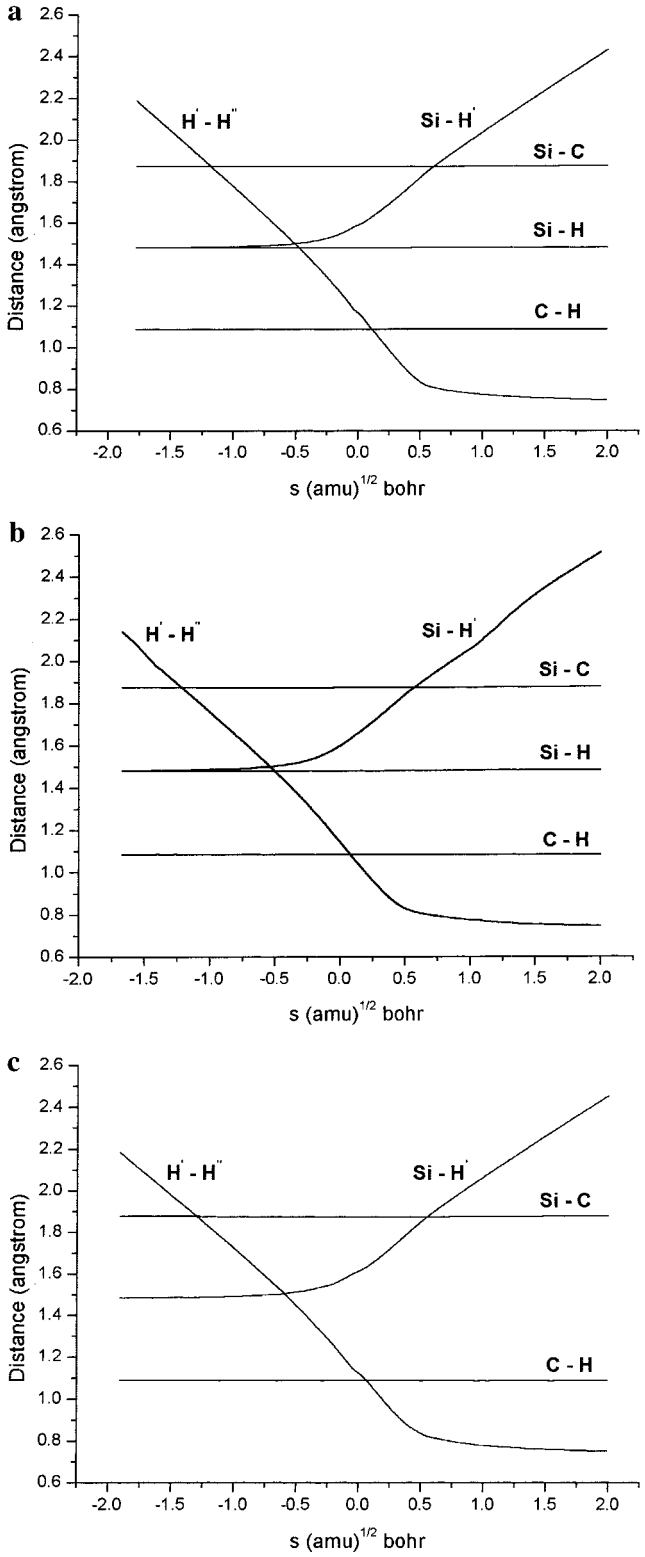

Figure 1. (a) Changes of the bond lengths (in angstroms) for the $SiH_3CH_3 + H \rightarrow SiH_2CH_3 + H_2$ reaction as functions of s [$(amu)^{1/2}$ bohr] at the BHLYP/6-311+G** level. (b) Same as those in (a) except for the $SiH_2(CH_3)_2 + H \rightarrow SiH(CH_3)_2 + H_2$ reaction. (c) Same as those in (a) except for the $SiH(CH_3)_3 + H \rightarrow Si(CH_3)_3 + H_2$ reaction.

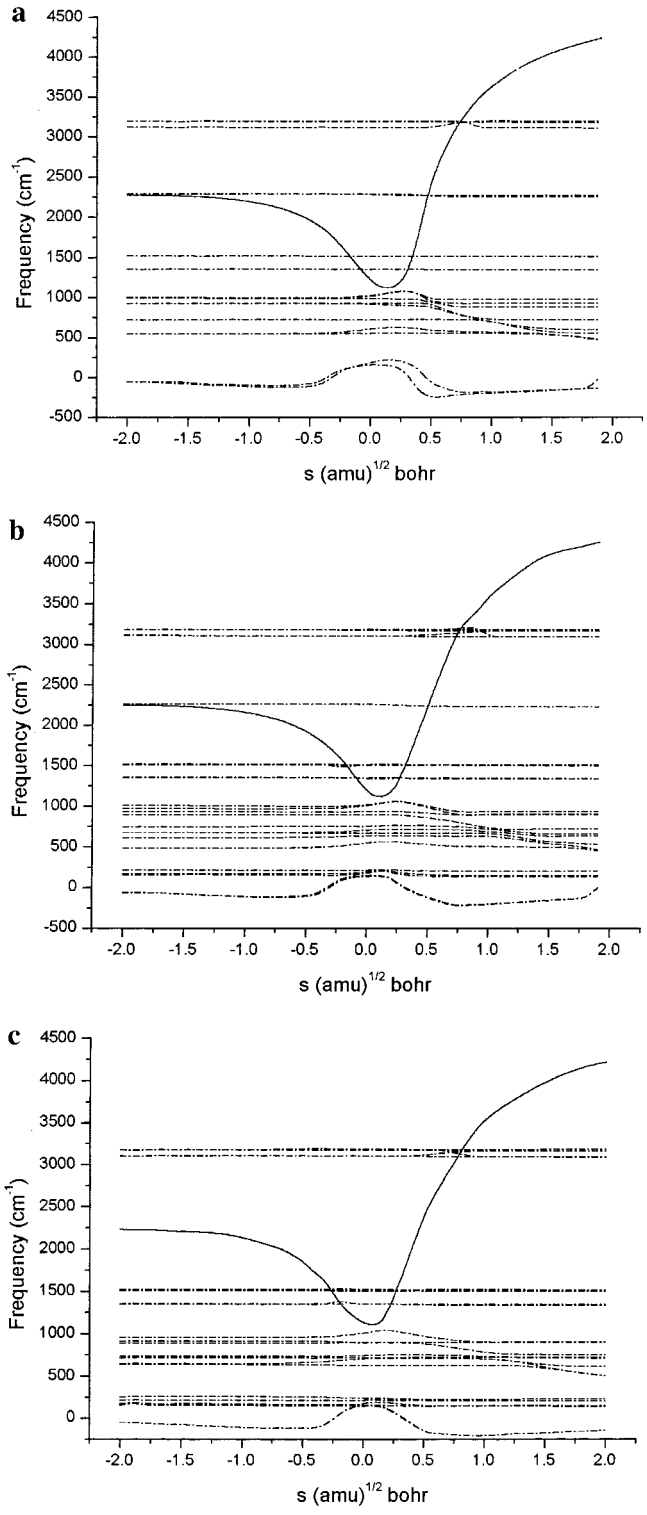

Figure 2. (a) Changes of the generalized normal-mode vibrational frequencies for the $SiH_3CH_3 + H \rightarrow SiH_2CH_3 + H_2$ reaction as functions of s [(amu)$^{1/2}$ bohr] at the BHLYP/6-311+G** level. (b) Same as those in (a) except for the $SiH_2(CH_3)_2 + H \rightarrow SiH(CH_3)_2 + H_2$ reaction. (c) Same as those in (a) except for the $SiH(CH_3)_3 + H \rightarrow Si(CH_3)_3 + H_2$ reaction.

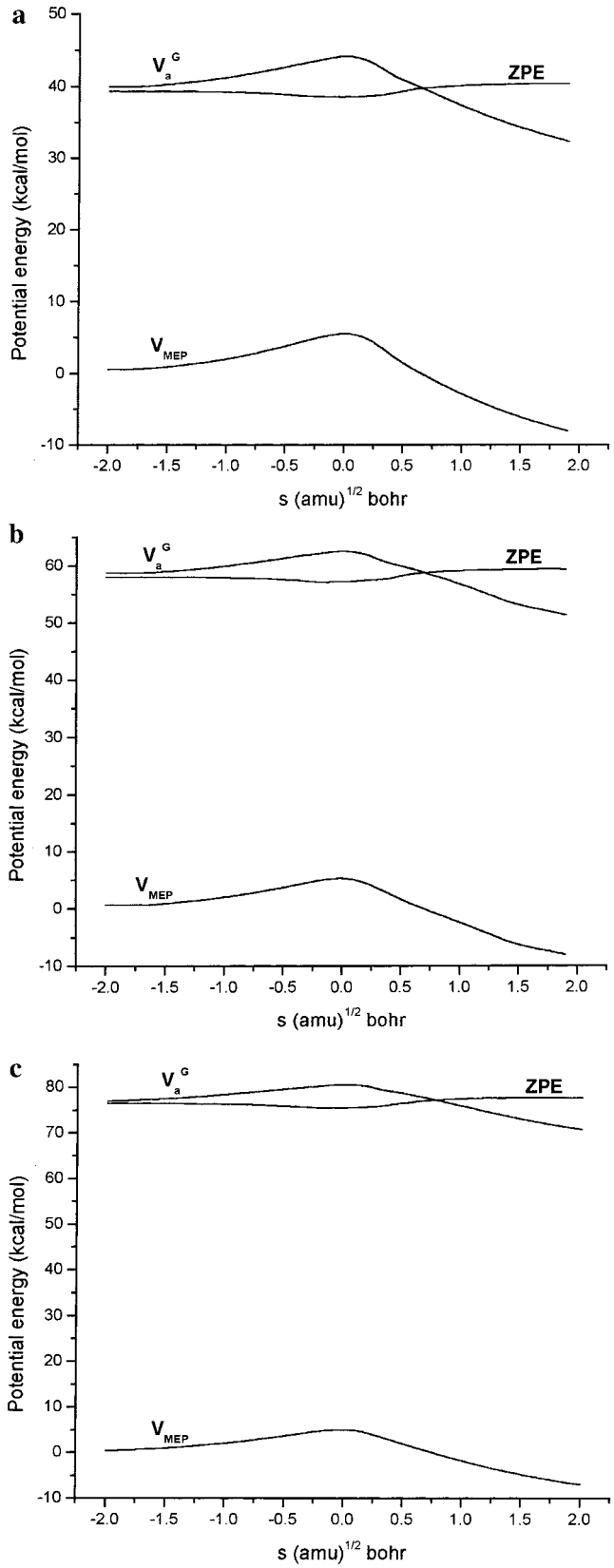

Figure 3. (a) Classical potential energy (V_{MEP}), zero-point energy (ZPE), and ground-state vibrationally adiabatic potential energy (V_a^G) for the $SiH_3CH_3 + H \rightarrow SiH_2CH_3 + H_2$ reaction as functions of s [(amu)$^{1/2}$ bohr] at the PMP4/6-311+G(3df,2p)//BHLYP level. (b) Same as those in (a) except for the $SiH_2(CH_3)_2 + H \rightarrow SiH(CH_3)_2 + H_2$ reaction. (c) Same as those in (a) except for the $SiH(CH_3)_3 + H \rightarrow Si(CH_3)_3 + H_2$ reaction.

tion that the BHLYP method underestimates the potential-barrier height has also been found in the studies of other reactions.[16−18] It is suggested that the underestimated potential barriers at the BHLYP/6-311+G** level will lead to overestimated rate constants of the reactions.

In conclusion, we find that the BHLYP/6-311+G** level can provide accurate geometry and frequency information, and additional PMP4/6-311+G(3df,2p)//BHLYP calculations can be utilized effectively to improve the potential energy.

TABLE 4: Rate Constants ($cm^3\ mol^{-1}\ s^{-1}$) for the Reactions of H Atoms with $SiH_{4-n}(CH_3)_n$, $n = 1-3$, Respectively, in the Temperature Range 290−3000 K at the PMP4/6-311+G(3df,2p)//BHLYP Level

$SiH_3CH_3 + H \rightarrow SiH_2CH_3 + H_2$					$SiH_2(CH_3)_2 + H \rightarrow SiH(CH_3)_2 + H_2$					$SiH(CH_3)_3 + H \rightarrow Si(CH_3)_3 + H_2$				
T, K	TST	CVT	CVT/SCT	exptl[a]	*T*, K	TST	CVT	CVT/SCT	exptl[a]	*T*, K	TST	CVT	CVT/SCT	exptl[a]
291	9.94×10^9	8.97×10^9	6.57×10^{10}		292	1.25×10^{10}	1.14×10^{10}	6.44×10^{10}		290	1.10×10^{10}	1.01×10^{10}	3.79×10^{10}	
298	1.23×10^{10}	1.10×10^{10}	7.41×10^{10}	2.33×10^{11}	298	1.48×10^{10}	1.36×10^{10}	7.17×10^{10}	2.38×10^{11}	298	1.37×10^{10}	1.25×10^{10}	4.38×10^{10}	1.67×10^{11}
321	2.31×10^{10}	2.06×10^{10}	1.08×10^{11}	3.72×10^{11}	321	2.70×10^{10}	2.45×10^{10}	1.05×10^{11}	3.76×10^{11}	334	3.25×10^{10}	2.93×10^{10}	7.95×10^{10}	2.87×10^{11}
341	3.75×10^{10}	3.32×10^{10}	1.46×10^{11}	5.46×10^{11}	343	4.49×10^{10}	4.04×10^{10}	1.46×10^{11}	4.88×10^{11}	366	6.14×10^{10}	5.52×10^{10}	1.26×10^{11}	4.22×10^{11}
367	6.57×10^{10}	5.76×10^{10}	2.10×10^{11}	6.93×10^{11}	365	7.05×10^{10}	6.26×10^{10}	1.98×10^{11}	6.81×10^{11}	410	1.29×10^{11}	1.14×10^{11}	2.17×10^{11}	6.44×10^{11}
390	1.02×10^{11}	8.85×10^{10}	2.81×10^{11}	8.67×10^{11}	387	1.05×10^{11}	9.34×10^{10}	2.61×10^{11}	7.83×10^{11}	455	2.39×10^{11}	2.10×10^{11}	3.52×10^{11}	9.22×10^{11}
444	2.42×10^{11}	2.09×10^{11}	5.13×10^{11}	1.49×10^{12}	418	1.75×10^{11}	1.54×10^{11}	3.73×10^{11}	1.03×10^{12}	494	3.78×10^{11}	3.29×10^{11}	5.08×10^{11}	1.20×10^{12}
479	3.87×10^{11}	3.32×10^{11}	7.23×10^{11}	1.86×10^{12}	458	3.07×10^{11}	2.67×10^{11}	5.63×10^{11}	1.48×10^{12}	499	3.99×10^{11}	3.48×10^{11}	5.31×10^{11}	1.24×10^{12}
505	5.29×10^{11}	4.52×10^{11}	9.09×10^{11}	2.09×10^{12}	508	5.56×10^{11}	4.80×10^{11}	8.79×10^{11}	2.22×10^{12}	540	6.02×10^{11}	5.22×10^{11}	7.17×10^{11}	1.36×10^{12}
580	1.14×10^{12}	9.58×10^{11}	1.63×10^{12}	2.85×10^{12}	551	8.61×10^{11}	7.41×10^{11}	1.23×10^{12}	2.72×10^{12}	579	8.55×10^{11}	7.35×10^{11}	9.58×10^{11}	1.79×10^{12}
600	1.36×10^{12}	1.14×10^{12}	1.87×10^{12}		580	1.12×10^{12}	9.58×10^{11}	1.51×10^{12}	3.17×10^{12}	580	8.61×10^{11}	7.41×10^{11}	9.64×10^{11}	1.73×10^{12}
800	5.29×10^{12}	4.34×10^{12}	5.67×10^{12}		800	4.92×10^{12}	4.07×10^{12}	5.09×10^{12}		800	3.58×10^{12}	2.94×10^{12}	3.29×10^{12}	
1000	1.31×10^{13}	1.06×10^{13}	1.25×10^{13}		1000	1.18×10^{13}	9.58×10^{12}	1.09×10^{13}		1000	8.37×10^{12}	6.69×10^{12}	7.05×10^{12}	
1200	2.55×10^{13}	2.04×10^{13}	2.26×10^{13}		1200	2.26×10^{13}	1.80×10^{13}	1.95×10^{13}		1200	1.57×10^{13}	1.23×10^{13}	1.26×10^{13}	
1400	4.29×10^{13}	3.40×10^{13}	3.64×10^{13}		1400	3.73×10^{13}	2.95×10^{13}	3.08×10^{13}		1400	2.56×10^{13}	1.98×10^{13}	1.99×10^{13}	
1600	6.50×10^{13}	5.14×10^{13}	5.39×10^{13}		1600	5.63×10^{13}	4.39×10^{13}	4.51×10^{13}		1600	3.81×10^{13}	2.91×10^{13}	2.91×10^{13}	
1800	9.28×10^{13}	7.23×10^{13}	7.47×10^{13}		1800	7.89×10^{13}	6.14×10^{13}	6.20×10^{13}		1800	5.32×10^{13}	4.02×10^{13}	4.00×10^{13}	
2000	1.25×10^{14}	9.76×10^{13}	9.94×10^{13}		2000	1.06×10^{14}	8.13×10^{13}	8.19×10^{13}		2000	7.05×10^{13}	5.31×10^{13}	5.26×10^{13}	
2200	1.61×10^{14}	1.25×10^{14}	1.28×10^{14}		2200	1.36×10^{14}	1.04×10^{14}	1.04×10^{14}		2200	9.03×10^{13}	6.75×10^{13}	6.69×10^{13}	
2400	2.03×10^{14}	1.57×10^{14}	1.59×10^{14}		2400	1.70×10^{14}	1.29×10^{14}	1.29×10^{14}		2400	1.13×10^{14}	8.37×10^{13}	8.25×10^{13}	
2600	2.49×10^{14}	1.92×10^{14}	1.93×10^{14}		2600	2.08×10^{14}	1.57×10^{14}	1.56×10^{14}		2600	1.37×10^{14}	1.01×10^{14}	1.00×10^{14}	
2800	2.99×10^{14}	2.30×10^{14}	2.26×10^{14}		2800	2.49×10^{14}	1.88×10^{14}	1.86×10^{14}		2800	1.63×10^{14}	1.20×10^{14}	1.19×10^{14}	
3000	3.53×10^{14}	2.70×10^{14}	2.66×10^{14}		3000	2.93×10^{14}	2.20×10^{14}	2.17×10^{14}		3000	1.92×10^{14}	1.40×10^{14}	1.39×10^{14}	

[a] From ref 9.

B. Reaction Path Properties. The minimum energy paths of the reactions are calculated at the BHLYP/6-311+G** level by the IRC method. The energies of the MEP are further refined at the PMP4/6-311+G(3df,2p)//BHLYP level. For all the reactions the maximum position for the potential energy curve ($V_{MEP}(s)$) at the PMP4/6-311+G(3df,2p)//BHLYP level corresponds to the saddle-point structure at the BHLYP/6-311+G** level; therefore, the shifting of the maximum position for the $V_{MEP}(s)$ caused by the computational technique is avoided. Parts a−c of Figure 1 show the bond-length changes along the MEP of the reactions as functions of the intrinsic reaction coordinate *s* [(amu)$^{1/2}$ bohr] at the BHLYP/6-311+G** level. It can be seen that the changes are very similar for all the reactions. First, while the lengths of breaking bond Si−H′ and the forming bond H′−H″ change strongly in the course of the reaction, the other bond lengths do not change. Second, the Si−H′ bond distance remains insensitive up to $s = -0.5$ (amu)$^{1/2}$ bohr and then increases smoothly. Meanwhile, the H′−H″ distance rapidly shortens from reactants and arrives at the equilibrium bond length of the hydrogen molecule at about $s = 0.5$ (amu)$^{1/2}$ bohr. Therefore, the geometrical changes mainly take place in the region from about $s = -0.5$ to $+0.5$ (amu)$^{1/2}$ bohr.

Parts a−c of Figure 2 show the changes of the generalized normal-mode vibrational frequencies along the MEP for the reactions as functions of the intrinsic reaction coordinate s (amu)$^{1/2}$ bohr at the BHLYP/6-311+G** level. In the limit of negative *s*, the frequencies are associated with the reactants $SiH_3CH_3 + H$, $SiH_2(CH_3)_2 + H$, and $SiH(CH_3)_3 + H$, respectively, and in the limit of positive *s*, the frequencies are associated with the products $SiH_2CH_3 + H_2$, $SiH(CH_3)_2 + H_2$, and $Si(CH_3)_3 + H_2$, respectively. In the vicinity of the transition state, there are 21, 30, and 39 vibrational frequencies, respectively. The solid line as shown in each of Figure 2a−c signifies that the harmonic Si−H′ stretching vibrational frequency, corresponding to the generalized normal mode that breaks during the reaction, drops dramatically near the saddle point, and this mode correlates with H′−H″ stretch in the product region. This kind of behavior is known to be typical of hydrogen abstraction reactions. The two lowest harmonic frequencies corresponding to free rotations and translations of the reactants evolve to vibrations at about $s = -0.25$ (amu)$^{1/2}$ bohr, and they present a maximum near the saddle point.

Parts a−c of Figure 3 depict the classical potential energy (V_{MEP}), the zero-point energy (ZPE), and the ground-state vibrationally adiabatic potential energy (V_a^G) for the reactions as functions of the intrinsic reaction coordinate s (amu)$^{1/2}$ bohr at the PMP4/6-311+G(3df,2p)//BHLYP level. It can be seen that for all the reactions the maximum position for $V_{MEP}(s)$ and $V_a^G(s)$ energy curves is the same, and the two curves are similar in shape. This implies that the variational effect for the reactions will be small or almost negligible. In addition, from SiH_3CH_3 to $SiH(CH_3)_3$, with the complexity of the structures, the ZPE increases gradually, which results in the increase of V_a^G for the reactions.

C. Rate Constant Calculation. The rate constants of the reactions are calculated by canonical variational transition state theory with the small-curvature tunneling correction (CVT/SCT) method at the PMP4/6-311+G(3df,2p)//BHLYP level within 290−3000 K, and the results are listed in Table 4. Both the conventional transition state theory (TST) and the canonical variational transition state theory (CVT) rate constants are also calculated for comparison in the same temperature range, and the results are also listed in Table 4. For each of the reactions, the difference between the values of TST rate constants and those of CVT rate constants in the whole temperature range is small, which enables us to conclude that the variational effect is small for the reactions. Also, in comparison with the rate constants of TST and CVT in the experimentally measured temperature ranges, the CVT/SCT rate constants are in much better agreement with the corresponding experimental values for the reactions. However, in the higher temperature ranges, the CVT/SCT rate constants are close to the rate constants of TST and CVT, which means only in the lower temperature ranges does the small-curvature tunneling (SCT) correction play an important role for the reactions. For example, for the $SiH_3CH_3 + H \rightarrow SiH_2CH_3 + H_2$ reaction, at 298 K the experimental rate constants are 18.9, 21.2, and 3.1 times as large as the calculated ones derived from the TST, CVT, and CVT/SCT methods, respectively. At 580 K, the multiplying factors are 2.5, 3.0, and 1.7, respectively. In addition, the tunneling effect

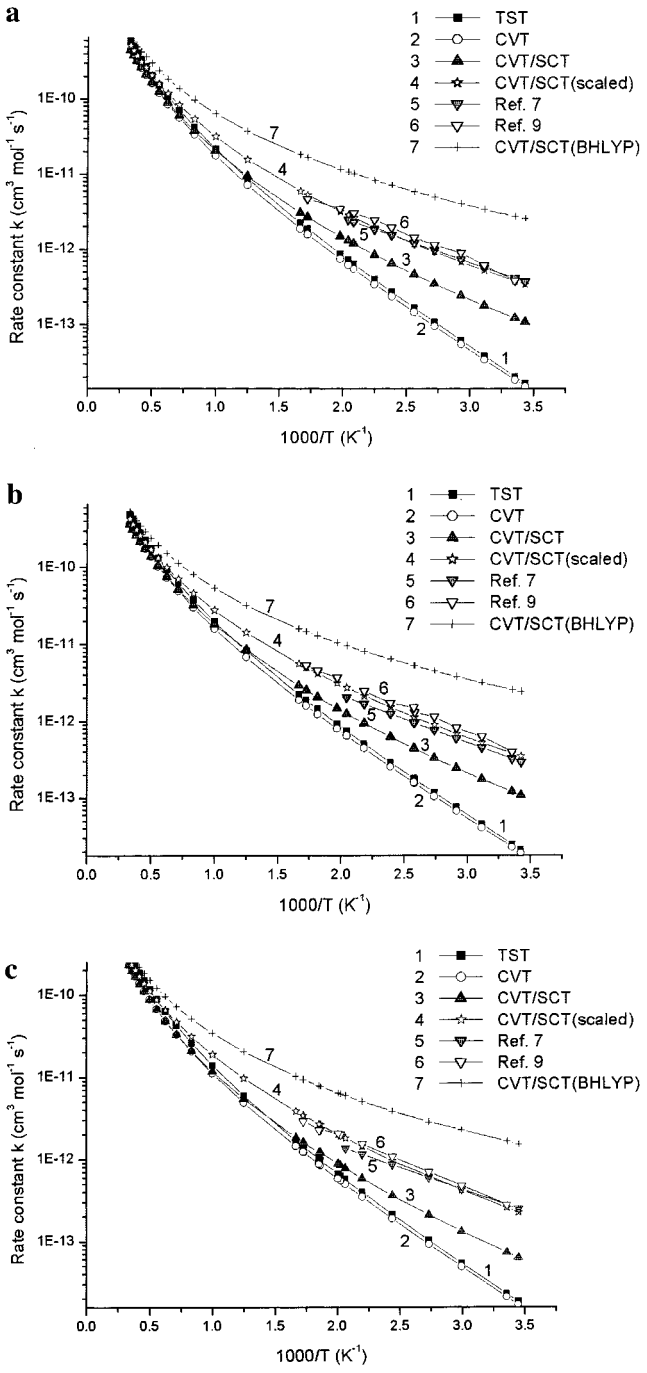

Figure 4. (a). Plot of the calculated rate constants k (cm^3 mol^{-1} s^{-1}) at the PMP4/6-311+G(3df,2p)//BHLYP level, CVT/SCT rate constants at the BHLYP/6-311+G** level, and the available experimental data vs 1000/T in 290−3000 K for the $SiH_3CH_3 + H \rightarrow SiH_2CH_3 + H_2$ reaction. (b). Same as those in (a) except for the $SiH_2(CH_3)_2 + H \rightarrow SiH(CH_3)_2 + H_2$ reaction. (c). Same as those in (a) except for the $SiH(CH_3)_3 + H \rightarrow Si(CH_3)_3 + H_2$ reaction.

is similar over the entire calculated temperature ranges for the three reactions. The same results can be seen clearly from Figure 4a−c that plot the theoretical and available experimental rate constants[7,9] for the reactions against 1000/T within 290−3000 K. The CVT/SCT rate constants calculated at the BHLYP/6-311+G** level overestimate the rate constants for the three reactions, which can be seen also from Figure 4a−c. Notice that even at the PMP4/6-311+G(3df,2p)//BHLYP level, there is still a little discrepancy between the CVT/SCT rate constants and experimental values for the reactions. The discrepancy is mainly from the inaccuracy of the PES apart from the semiclassical nature of the dynamics methodology. The best agreement of the theoretical rate constants with experiment is found for all the reactions if one tolerates the adjustment of the computed potential energy scaled by 0.83, 0.82, and 0.80, respectively, and the results are also plotted in Figure 4a−c. To provide the most possible comparison with experiment, the activation energies of the reactions are calculated at the PMP4/6-311+G(3df,2p)//BHLYP level in the experimentally measured temperature ranges, and the values of the three reactions are nearly the same, as shown in Table 5. The same trend has been found for the activation energies from the scaled potential energy curves, and the results are in good agreement with those of Arthur, Potzinger, and co-workers[7] and Arthur and Miles.[9] The maximum discrepancy is found to be 0.55 kcal/mol for $SiH(CH_3)_3$. Finally, we present three-parameter fits for rate constants of the reactions within 290−3000 K at the PMP4/6-311+G(3df,2p)//BHLYP level to describe the non-Arrhenius behavior of the rate constants in the broader temperature range. The expressions are $k(SiH_3CH_3 + H) = 4.5 \times 10^6 T^{2.29} \exp(-1000/T)$ cm^3 mol^{-1} s^{-1}, $k(SiH_2(CH_3)_2 + H) = 7.3 \times 10^6 T^{2.20} \exp(-1003/T)$ cm^3 mol^{-1} s^{-1}, and $k(SiH(CH_3)_3 + H) = 6.6 \times 10^6 T^{2.16} \exp(-1046/T)$ cm^3 mol^{-1} s^{-1}.

TABLE 5: Activation Energies (in kcal/mol) for the Reactions

reaction	T, K	PMP4//BHLYP	PMP4//BHLYP (scaled)	exptl
$SiH_3CH_3 + H \rightarrow SiH_2CH_3 + H_2$	291−489	3.56	3.02	2.70[a]
	298−580	3.76	3.20	3.15[b]
$SiH_2(CH_3)_2 + H \rightarrow SiH(CH_3)_2 + H_2$	292−489	3.52	2.97	2.80[a]
	298−580	3.71	3.14	3.15[b]
$SiH(CH_3)_3 + H \rightarrow Si(CH_3)_3 + H_2$	290−485	3.61	2.99	2.44[a]
	298−580	3.76	3.16	2.80[b]

[a] From ref 7. [b] From ref 9.

TABLE 6: Effect of Methyl Substitution on the Reactivity of the Si−H Bond in Silanes

no. of Si−H bonds	$10^{13}k/n$ (298 K), cm^3 s^{-1}			$10^{11}A/n$, cm^3 s^{-1}				E_a, kcal mol^{-1}			
	ref 7	ref 9	this work	ref 7	ref 9	this work		ref 7	ref 9	this work	
3	1.33	1.29	1.28	1.3	2.86	2.04[a]	2.53[b]	2.70	3.15	3.02[a]	3.20[b]
2	1.55	1.98	1.89	1.8	3.94	2.68[a]	3.52[b]	2.80	3.15	2.97[a]	3.14[b]
1	2.60	2.78	2.56	1.7	3.29	3.76[a]	5.06[b]	2.44	2.80	2.99[a]	3.16[b]

[a] In the same temperature range as ref 7. [b] In the same temperature range as ref 9.

D. Reactivity Trends. The effect of increasing methyl substitution on the reactivity of the Si−H bond is evaluated by the present reaction systems of H atoms with $SiH_{4-n}(CH_3)_n$, $n = 1-3$, and the results are compared in Table 6. The data of "this work" are the results based on the scaled MEP at the PMP4/6-311+G(3df,2p)//BHLYP level. k/n is the value of the rate constant at 298 K corrected for reaction path degeneracy, A/n is the A factor, similarly corrected, and n is the number of Si−H bonds. From our calculational results, one can see that methyl substitution leads to an increase in the Si−H bond reactivity, and the increase in k/n along the series mainly stems from a corresponding increase in A/n. The activation energies for the three reactions are nearly the same, which is consistent with the expectation of Arthur, Potzinger, and co-workers,[7] while the calculated values of k/n are much closer to those of the most recent work by Arthur and Miles.[9]

Conclusions

In this paper, the three hydrogen abstraction reactions of H atoms with different methylsilanes, $SiH_{4-n}(CH_3)_n$, $n = 1-3$,

have been investigated by DFT and ab initio direct dynamics methods. The results show that methyl substitution leads to an increase in the Si−H bond reactivity, and the increase in k/n mainly stems from a corresponding increase in A/n. The activation energies for the three reactions are nearly the same. The BHLYP/6-311+G** method can provide accurate geometry and frequency information, and the series of single-point calculations of PMP4/6-311+G(3df,2p)//BHLYP are essential to improve the potential energy curves of the reactions. The CVT/SCT rate constants at the PMP4/6-311+G(3df,2p)//BHLYP level are in good agreement with the experimental ones in the experimentally measured temperature ranges. The variational effect is small, and the small curvature tunneling effect is important for the reactions in the lower temperature ranges. The three-parameter fits for rate constants of the reactions within 290−3000 K are $k(SiH_3CH_3 + H) = 4.5 \times 10^6 T^{2.29} \exp(-1000/T)$ cm^3 mol^{-1} s^{-1}, $k(SiH_2(CH_3)_2 + H) = 7.3 \times 10^6 T^{2.20} \exp(-1003/T)$ cm^3 mol^{-1} s^{-1}, and $k(SiH(CH_3)_3 + H) = 6.6 \times 10^6 T^{2.16} \exp(-1046/T)$ cm^3 mol^{-1} s^{-1}.

Acknowledgment. We thank Professor Donald G. Truhlar for providing the POLYRATE 8.4.1 program. This work is supported by the National Science Foundation of China (project No. 29892168).

References and Notes

(1) Ding, L.; Marshall, P. *J. Am. Chem. Soc.* **1992**, *114*, 5754.
(2) Ding, L.; Marshall, P. *J. Phys. Chem.* **1992**, *96*, 2197.
(3) Doncaster, A. M.; Walsh, R. *J. Chem. Soc., Faraday Trans. 1* **1979**, *75*, 1126.
(4) Arthur, N. L.; Bell, T. N. *Rev. Chem. Intermed.* **1978**, *2*, 37.
(5) Horie, O.; Taege, R.; Reimann, B.; Arthur. N. L.; Potzinger, P. *J. Phys. Chem.* **1991**, *95*, 4393.
(6) Austin, E. R.; Lampe, F. W. *J. Phys. Chem.* **1977**, *81*, 1134.
(7) Arthur, N. L.; Potzinger, P.; Reimann, B.; Steenbergen, H.-P. *J. Chem. Soc., Faraday Trans. 2* **1989**, *85*, 1447.
(8) Arthur, N. L.; Miles, L. A. *Chem. Phys. Lett.* **1998**, *282*, 192.
(9) Arthur, N. L.; Miles, L. A. *J. Chem. Soc., Faraday Trans.* **1998**, *94*, 1077.
(10) Duncan, W. T.; Truong, T. N. *J. Chem. Phys.* **1995**, *103*, 9642.
(11) Bell, R. L.; Truong, T. N. *J. Chem. Phys.* **1994**, *101*, 10442.
(12) Truong, T. N. *J. Chem. Phys.* **1995**, *102*, 5335.
(13) Truong, T. N.; Evans, T. J. *J. Phys. Chem.* **1994**, *98*, 9558.
(14) Truong, T. N.; Duncan, W. T.; Bell, R. L. In *Chemical Applications of Density-Functional Theory*; American Chemical Society: Washington, DC, 1996; p 85.
(15) Maity, D. K.; Duncan, W. T.; Truong, T. N. *J. Phys. Chem. A* **1999**, *103*, 2152.
(16) Duncan, W. T. Ph.D. Thesis, University of Utah, 1999.
(17) Li, S.-M.; Yu, X.; Xu, Z.-F.; Li, Z.-S.; Sun, C.-C. *J. Phys. Chem. A.* **2001**, *105*, 3967.
(18) Yu, X.; Li, S.-M.; Xu, Z.-F.; Li, Z.-S.; Sun, C.-C. *J. Mol. Struct. (THEOCHEM)* **2001**, *543*, 11.
(19) Truhlar, D. G.; Gordon, M. S. *Science* **1990**, *249*, 491.
(20) Frisch, M. J.; Trucks, G. W.; Schlegel, H. B.; Scuseria, G. E.; Robb, M. A.; Cheeseman, J. R.; Zakrzewski, V. G.; Montgomery, J. A., Jr.; Stratmann, R. E.; Burant, J. C.; Dapprich, S.; Millam, J. M.; Daniels, A. D.; Kudin, K. N.; Strain, M. C.; Farkas, O.; Tomasi, J.; Barone, V.; Cossi, M.; Cammi, R.; Mennucci, B.; Pomelli, C.; Adamo, C.; Clifford, S.; Ochterski, J.; Petersson, G. A.; Ayala, P. Y.; Cui, Q.; Morokuma, K.; Malick, D. K.; Rabuck, A. D.; Raghavachari, K.; Foresman, J. B.; Cioslowski, J.; Ortiz, J. V.; Baboul, A. G.; Stefanov, B. B.; Liu, G.; Liashenko, A.; Piskorz, P.; Komaromi, I.; Gomperts, R.; Martin, R. L.; Fox, D. J.; Keith, T.; Al-Laham, M. A.; Peng, C. Y.; Nanayakkara, A.; Gonzalez, C.; Challacombe, M.; Gill, P. M. W.; Johnson, B.; Chen, W.; Wong, M. W.; Andres, J. L.; Gonzalez, C.; Head-Gordon, M.; Replogle, E. S.; Pople, J. A. *Gaussian98*; Gaussian, Inc.: Pittsburgh, PA, 1998.
(21) Chuang, Y.-Y.; Corchado, J. C.; Fast, P. L.; Villa, J.; Hu, W.-P.; Liu, Y.-P.; Lynch, G. C.; Jackels, C. F.; Nguyen, K. A.; Gu, M. Z.; Rossi, I.; Coitino, E. L.; Clayton, S.; Melissas, V. S.; Lynch, B. J.; Steckler, R.; Garrett, B. C.; Isaacson, A. D.; Truhlar, D. G. *POLYRATE*, version 8.4.1; University of Minnesota: Minneapolis, 2000.
(22) Truhlar, D. G.; Isaacson, A. D.; Garret, B. C. In *Theory of Chemical Reaction Dynamics*; Baer, M., Ed.; CRC Press: Boca Raton, FL, 1985; p 65.
(23) Steckler, R.; Hu, W.-P.; Liu, Y.-P.; Lynch, G. C.; Garrett, B. C.; Isaacson, A. D.; Melissas, V. S.; Lu, D.-H.; Troung, T. N.; Rai, S. N.; Hancock, G. C.; Lauderdale, J. G.; Joseph, T.; Truhlar, D. G. *Comput. Phys. Commun.* **1995**, *88*, 341.
(24) Lide, D. R. In *CRC Handbook of Chemistry and Physics*, 73rd ed.; CRC Press: Boca Raton, FL, 1992.
(25) Shimanouchi, T. *Tables of Molecular Vibrational Frequencies Consolidated*; National Bureau of Standards: Washington, DC, 1972; Vol. I.